Functional Models for Catechol 1,2-Dioxygenase. The Role of the Iron(III) Center

David D. Cox and Lawrence Que, Jr.*

Contribution from the Department of Chemistry, University of Minnesota, Minneapolis, Minnesota 55455. *Received April 4, 1988*

Abstract: A series of [Fe(L)DBC] complexes, where L is a tetradentate tripodal ligand and DBC is 3,5-di-*tert*-butylcatecholate, has been prepared to serve as functional mimics for the catechol dioxygenases. The tripodal ligands, $(RCH_2)_2N(CH_2R')$ (NTA, R = R' = COO^-; PDA, R = COO^-, R' = 2-pyridyl; BPG, R = 2-pyridyl, R' = COO^-; HDP, R = 2-pyridyl, R' = 2-hydroxy-3,5-dimethylphenyl), serve to tune the Lewis acidity of the ferric center. This tuning is manifested in differences in the energies of the catecholate-to-Fe^{III} charge-transfer bands, the potentials of the semiquinone/catecholate couple, and the shifts of the DBC protons found for the complexes. These complexes react with O_2 with high specificity to yield a product resulting from C1-C2 oxidative cleavage. Kinetic studies show that the rate-determining step involves the attack of dioxygen on the complex, and the rates of reaction of the complexes increase in the order of HDP, NTA, PDA, and BPG. This order in general follows the increase in Lewis acidity of the ferric center but more specifically correlates with increasing semiquinone character on the DBC ligand as indicated by the NMR shifts. As a further check, $[Fe(BPG)DBC]\cdot 2CH_3OH$ ($P2_1/n$) was crystallographically characterized and compared with the previously reported $[Fe(NTA)DBC]^{2-}$. The structures are similar; both are six-coordinate high-spin ferric complexes with unsymmetrically chelated DBC ligands ($\Delta r_{Fe-O(DBC)} = 0.1$ Å for both). Taken together, these observations suggest that the substrate activation proposed for the dioxygenase mechanism results from the delocalization of unpaired spin density from the ferric center onto the coordinated catecholate arising from ligand-to-metal charge transfer.

Catechol 1,2-dioxygenase and protocatechuate 3,4-dioxygenase are non-heme iron enzymes that catalyze the oxidative cleavage of catechols of *cis,cis*-muconic acids with the incorporation of molecular oxygen.[1] On the basis of a variety of spectroscopic techniques, the active sites of these enzymes are proposed to consist of a high-spin ferric center[2] coordinated to two tyrosines,[3] two histidines,[4] and a water.[5] The reaction sequence involves initial substrate binding to the ferric center generating an iron(III)-catecholate complex[6] and subsequent attack by dioxygen on the enzyme-substrate complex. Spectroscopic studies indicate that the iron center remains high-spin ferric throughout this sequence.[2,7] We have proposed a substrate activation mechanism for this reaction, wherein coordination to the paramagnetic metal center renders the substrate susceptible to dioxygen attack because of the delocalization of unpaired spin density from the iron onto the catecholate.[8,9]

Model systems that mimic enzyme reactions are important mechanistic tools, because the flexibility in ligand design allows a systematic investigation of the important factors affecting reactivity. It is essential to fully characterize the complexes involved in the biomimetic reactions. Our efforts in this regard have been stimulated by the work of Weller and Weser[10] on the FeNTA[11]/borate buffer/DMF or MeOH system and Funabiki et al.[12]

Scheme I

Tripodal Ligands

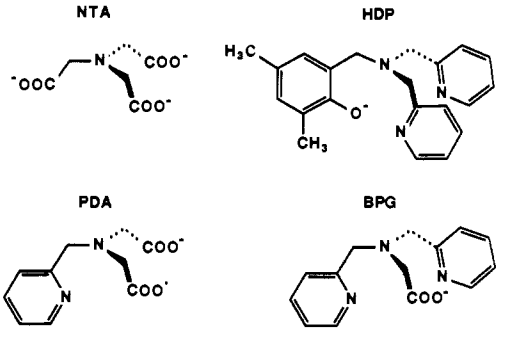

on the $FeCl_3$/bpy/pyridine system, because of the significant yields of cleavage products that can be obtained from these systems. In earlier work, we reported the physical and chemical properties of a series of ternary complexes, $[FeL(DBC)]^{2-}$, where L is a trianionic tripodal ligand, including the crystal structure of $[Fe(NTA)DBC]^{2-}$.[13] This study established that the Lewis acidity of the ferric center, as modulated by the tripodal ligand, played an important role in dictating the nature of the products and their yields. In the present study, we have extended our investigations to complexes of iron centers of even greater Lewis acidity. These complexes react with O_2 with faster rates and even higher specificity. A comparison of their spectroscopic and kinetic properties affords insights into the nature of the substrate activation in the proposed dioxygenase mechanism.

Experimental Section

Ligands. The ligands used in this study are shown in Scheme I. NTA and $DBCH_2$ were obtained from Aldrich, and the latter was further purified by recrystallization from hexane. $DBCH_2$-*4,6-d*$_2$ was prepared

(1) For recent reviews of these enzymes, see: Que, L., Jr. *Adv. Inorg. Biochem.* **1983**, *5*, 167-199. Que, L., Jr. *J. Chem. Educ.* **1985**, *62*, 938-942.
(2) (a) Que, L., Jr.; Lipscomb, J. D.; Zimmermann, R.; Münck, E.; Orme-Johnson, W. H.; Orme-Johnson, N. R. *Biochim. Biophys. Acta* **1976**, *452*, 320-334. (b) Whittaker, J. W.; Lipscomb, J. D.; Kent, T. A.; Münck, E. *J. Biol. Chem.* **1984**, *259*, 4466-4475. (c) Kent, T. A.; Münck, E.; Pyrz, J. W.; Widom, J.; Que, L., Jr. *Inorg. Chem.* **1987**, *26*, 1402-1408.
(3) (a) Que, L., Jr.; Heistand, R. H., II; Mayer, R.; Roe, A. L. *Biochemistry* **1980**, *19*, 2588-2593. (b) Que, L., Jr.; Epstein, R. M. *Biochemistry* **1981**, *20*, 2545-2549.
(4) Felton, R. H.; Barrow, W. L.; May, S. W.; Sowell, A. L.; Goel, S. *J. Am. Chem. Soc.* **1982**, *104*, 6132-6134.
(5) Whittaker, J. W.; Lipscomb, J. D. *J. Biol. Chem.* **1984**, *259*, 4487-4495.
(6) Que, L., Jr.; Heistand, R. H., II *J. Am. Chem. Soc.* **1979**, *101*, 2219-2221. Felton, R. H.; Cheung, L. D.; Phillips, R. S.; May, S. W. *Biochem. Biophys. Res. Commun.* **1978**, *85*, 844-850.
(7) (a) Bull, C.; Ballou, D. P.; Otsuka, S. *J. Biol. Chem.* **1981**, *256*, 12681-12686. (b) Walsh, T. A.; Ballou, D. P.; Mayer, R.; Que, L., Jr. *J. Biol. Chem.* **1983**, *258*, 14422-14427.
(8) Que, L., Jr.; Lipscomb, J. D.; Münck, E.; Wood, J. M. *Biochim. Biophys. Acta* **1977**, *485*, 60-74.
(9) Que, L., Jr.; Lauffer, R. B.; Lynch, J. B.; Murch, B. P.; Pyrz, J. W. *J. Am. Chem. Soc.* **1987**, *109*, 5381-5385.
(10) (a) Weller, M. G.; Weser, U. *J. Am. Chem. Soc.* **1982**, *104*, 3752-3754. (b) Weller, M. G.; Weser, U. *Inorg. Chim. Acta* **1985**, *107*, 243-245.

(11) Abbreviations used: NTA, nitrilotriacetate; $DBCH_2$, 3,5-di-*tert*-butylcatechol; DBSQ, 3,5-di-*tert*-butyl-*o*-benzosemiquinone; DBQ, 3,5-di-*tert*-butyl-*o*-benzoquinone; SCE, saturated calomel electrode; $catH_2$, catechol; bpy, 2,2'-bipyridyl; tpbn, *N,N,N',N'*-tetrakis(2-pyridylmethyl)-1,4-diaminobutane; XYL-O, 2,6-bis(((2-(2-pyridyl)ethyl)amino)methyl)-4-methylphenol; LMCT, ligand-to-metal charge transfer.
(12) (a) Funabiki, T.; Mizoguchi, A.; Sugimoto, T.; Tada, S.; Tsuji, M.; Sakamoto, H.; Yoshida, S. *J. Am. Chem. Soc.* **1986**, *108*, 2921-2932. (b) Funabiki, T.; Konishi, T.; Kobayashi, S.; Mizoguchi, A.; Takano, M.; Yoshida, S. *Chem. Lett.* **1987**, 719-722.
(13) Que, L., Jr.; Kolanczyk, R. C.; White, L. S. *J. Am. Chem. Soc.* **1987**, *109*, 5373-5380.

0002-7863/88/1510-8085$01.50/0

Table I. Crystallographic Data for [Fe(BPG)DBC]·2CH$_3$OH

formula	$C_{30}H_{42}FeN_3O_6$
MW	596.54
space group	$P2_1/n$
a, Å	11.803 (9)
b, Å	14.424 (7)
c, Å	17.656 (6)
α, deg	90.0
β, deg	101.2 (1)
γ, deg	90.0
V, Å^3	2948
Z	4
D_{calc}, g/cm^3	1.344
radiation used	Mo K$_\alpha$(λ = 0.71073 Å)
max [(sin θ)/λ]	0.62
crystal size, mm^3	0.20 × 0.30 × 0.55
μ, cm^{-1}	5.482
no. of reflcns measd	5784
reflcns used[a]	4110 [$(F_o)^2 \geq 1\sigma(F_o)^2$]
no. of variables used	398
R^b	0.050
$R_w{}^b$	0.058
GOF[b]	1.418
p[a]	0.05

[a] The intensity data were processed as described in: *CAD 4 and SDP-PLUS User's* Manual; B.A. Frenz & Assoc.: College Station, TX, 1982. The net intensity $I = [K(\mathrm{NPI})](C - 2B)$, where K = 20.1166 (attenuator factor), NPI = ratio of fastest possible scan rate to scan rate for the measurement, C = total count, and B = total background count. The standard deviation in the net intensity is given by $[\sigma(I)]^2 = (k/\mathrm{NPI})^2[C + 4B + (pI)^2]$ where p is a factor used to downweight intense reflections. The observed structure factor amplitude F_o is given by $F_o = (I/Lp)^{1/2}$, where Lp = Lorentz and polarization factors. The $\sigma(I)$'s were converted to the estimated errors in the relative structure factors $\sigma(F_o)$ by $\sigma(F_o) = 1/2[\sigma(I/I]F_o$. [b] The function minimized was $\sum w(|F_o| - |F_c|)^2$, where $w = 1/[\sigma(f_o)]^2$. The unweighted and weighted residuals are defined as $R = (||F_o| - |F_c||)/\sum|F_o|$ and $R_w = [(\sum w(|F_o| - |F_c|))^2/(\sum w|f_o|)^2]^{1/2}$. The error is an observation of unit weight. (GOF) is $[\sum w(|F_o| - |F_c|)^2/(\mathrm{NO} - \mathrm{NV})]^{1/2}$, where NO and NV are the number of observations and variables, respectively.

by deuterium exchange in D_2O in the presence of a substoichiometric amount of base at 140 °C in a sealed tube for 4 h.[14] PDA and BPG were prepared according to published procedures.[15]

2-[(Bis(2-pyridylmethyl)amino)methyl]-4,6-dimethylphenol (HDP) was synthesized by adding 1.0 g (5.4 mmol) of bis(picolyl)amine to 0.66 g (8.1 mmol) of 37% formalin in 5 mL of MeOH at 0 °C under nitrogen and then adding 1.1 g (5.4 mmol) of 2,4-dimethylphenol in 4 mL of MeOH dropwise. The solution was allowed to warm to room temperature and treated with 3 mL of HOAc. After the mixture was allowed to stir for 48 h, the solvent was removed under vacuum, neutralized with dilute NaOH, and extracted three times with 35 mL of CH_2Cl_2, and the organic layer was dried over Na_2SO_4. Thin-layer chromatography on silica gel with ethyl acetate as solvent yielded a spot with an R_f = 0.45. The crude mixture was then purified by flash chromatography on silica (after the methylene chloride was removed under reduced pressure) with ethyl acetate as eluant to afford 1.1 g (62%) of a pale yellow solid. ^{1}H NMR (acetone-d_6): 2.21 (s, 3 H), 2.26 (s, 3 H), 3.75 (s, 2 H), 3.85 (s, 4 H), 6.71 (s, 1 H), 6.86 (s, 1 H), 7.13–7.19 (m, 2 H), 7.34–7.38 (m, 2 H), 7.59–7.68 (m, 2 H), 8.57–8.59 (m, 2 H).

Complexes. The complexes (pipH)$_2$[Fe(NTA)DBC], (pipH)[Fe(PDA)DBC]·0.5H$_2$O, and [Fe(BPG)DBC] were prepared according to literature methods.[15]

[Fe(HDP)DBC]·H$_2$O was synthesized by heating 120 mg (0.25 mmol) of [Fe(HDP)Cl$_2$]·H$_2$O and 55.9 mg (0.25 mmol) of DBC in 15 mL of methanol under N_2 and then slowly adding 0.050 mL (0.50 mmol) of piperidine. Crystals were obtained upon cooling overnight. Anal. Calcd for $C_{35}H_{44}FeN_3O_4$: C, 67.09; H, 7.08; N, 6.71. Found: C, 66.93; H, 7.00; N, 6.82. [Fe(HDP)Cl$_2$]·H$_2$O was synthesized by the addition of 260 mg (0.78 mmol) of HDP·H$_2$O in 5 mL of hot methanol and 215 mg (0.78 mmol) of FeCl$_3$·6H$_2$O in 2 mL of methanol. Crystals formed upon standing. Anal. Calcd for $C_{21}H_{25}Cl_2FeN_3O_2$: C, 52.95; H, 5.27; N, 8.79. Found: C, 53.24; H, 5.20; N, 8.72. λ_{max} (MeOH) = 708 nm.

Table II. Atomic Coordinates for the Non-Hydrogen Atoms of [Fe(BPG)DBC]·2CH$_3$OH

atom	x	y	z	B, Å^2
Fe	0.20370 (4)	0.05917 (4)	0.13992 (3)	2.384 (8)
O1	0.1824 (2)	0.0515 (2)	0.2488 (1)	2.80 (4)
O2	0.0764 (2)	0.1408 (2)	0.1283 (1)	2.38 (4)
O3	0.2273 (2)	0.0636 (2)	0.0312 (1)	2.78 (5)
O4	0.3368 (2)	0.0124 (2)	−0.0507 (1)	3.40 (5)
N	0.3591 (2)	−0.0305 (2)	0.1557 (2)	2.70 (6)
N1B	0.3434 (2)	0.1554 (2)	0.1724 (2)	2.93 (6)
N1C	0.1342 (2)	−0.0778 (2)	0.1212 (2)	2.60 (6)
C1	0.4543 (3)	0.0156 (3)	0.2094 (2)	3.39 (8)
C2	0.3265 (3)	−0.1205 (3)	0.1859 (2)	2.99 (7)
C3	0.3867 (3)	−0.0410 (3)	0.0768 (2)	3.14 (7)
C4	0.3119 (3)	0.0164 (3)	0.0139 (2)	2.71 (6)
C1A	0.0933 (3)	0.1064 (2)	0.2589 (2)	2.44 (6)
C2A	0.0366 (3)	0.1563 (2)	0.1942 (2)	2.23 (6)
C3A	0.0546 (3)	0.2161 (2)	0.1998 (2)	2.17 (6)
C4A	−0.0889 (3)	0.2217 (2)	0.2720 (2)	2.42 (6)
C5A	−0.0370 (3)	0.1693 (2)	0.3362 (2)	2.52 (6)
C6A	0.0550 (3)	0.1126 (3)	0.3286 (2)	2.61 (7)
C31	−0.1167 (3)	0.2700 (2)	0.1288 (2)	2.34 (6)
C32	−0.0289 (3)	0.3271 (3)	0.0944 (2)	2.84 (7)
C33	−0.1788 (3)	0.2007 (3)	0.0685 (2)	2.83 (7)
C34	−0.2070 (3)	0.3372 (3)	0.1475 (2)	3.35 (7)
C51	−0.0824 (3)	0.1715 (3)	0.4120 (2)	2.90 (7)
C52	0.0190 (6)	0.1820 (5)	0.4797 (3)	3.9 (1)
C53	−0.1413 (6)	0.0786 (6)	0.4197 (4)	5.4 (2)
C54	−0.1663 (6)	0.2502 (6)	0.4148 (4)	5.3 (2)
C52′	−0.0376 (9)	0.0913 (8)	0.4679 (5)	4.4 (2)
C53′	−0.2142 (8)	0.1661 (9)	0.3966 (5)	4.2 (2)
C54′	−0.0458 (9)	0.2617 (9)	0.4552 (6)	4.9 (3)
C2B	0.4487 (3)	0.1188 (3)	0.2007 (2)	3.11 (7)
C3B	0.5434 (3)	0.1758 (3)	0.2248 (2)	3.84 (9)
C4B	0.5296 (3)	0.2707 (3)	0.2226 (2)	4.42 (9)
C5B	0.4211 (3)	0.3077 (3)	0.1927 (2)	3.95 (9)
C6B	0.3314 (3)	0.2481 (3)	0.1683 (2)	3.36 (8)
C2C	0.2066 (3)	−0.1483 (3)	0.1459 (2)	2.69 (6)
C3C	0.1705 (3)	−0.2396 (3)	0.1376 (2)	3.03 (7)
C4C	0.0561 (3)	−0.2587 (3)	0.1041 (2)	3.26 (7)
C5C	−0.0172 (3)	−0.1863 (3)	0.0792 (2)	3.13 (7)
C6C	0.0236 (3)	−0.0970 (3)	0.0881 (2)	2.86 (7)

[Ga(BPG)DBC]·CH$_3$OH·H$_2$O was synthesized by warming 200 mg (0.78 mmol) of BPG and 198.7 mg (ca. 0.78 mmol) of Ga(NO$_3$)$_3$·xH$_2$O in 20 mL of methanol under N_2. After 30 min 173 mg (0.78 mmol) of DBC was added under N_2, along with the slow addition of 0.23 mL (2.33 mmol) of piperidine. A light yellow powder formed upon cooling. Anal. Calcd for $C_{29}H_{40}GaN_3O_6$: C, 58.41; H, 6.76; N, 7.05. Found: C, 58.24; H, 6.82; N, 7.34.

Crystallographic Studies. Crystals of [Fe(BPG)DBC]·2CH$_3$OH in the shape of parallelepipeds were obtained from a methylene chloride solution layered with toluene. The methanols of crystallization appear to be derived from the initial isolation of the complex from methanol. X-ray diffraction data were collected on an Enraf-Nonius CAD4 X-ray diffractometer with Mo Kα (λ = 0.71069 Å) radiation out to 2ϑ = 52°. Crystallographic data can be found in Table I. The structure was solved by Patterson and Fourier methods and refined anisotropically to a final value of R_1 of 0.050. The final difference map did not reveal any chemically significant electron density; the most intense peak corresponded to a hydrogen of a CH_3 group on one of the methanols having a density of 0.48 e/Å^3.

An ORTEP plot of the structure is shown in Figure 1, together with the numbering scheme for the complex. Atomic coordinates for the non-hydrogen atoms for [Fe(BPG)DBC]·2CH$_3$OH and selected bond distances and bond angles are given in Tables II and III, respectively; atomic coordinates for the hydrogen atoms of the complex and the solvent molecules and their thermal parameters can be found in Tables S-1 and S-2 (supplementary material).

Accuracy in this structure (R = 5.0 and R_w = 5.8) is limited by some disorder present in the 5-*tert*-butyl group on the catechol. The *tert*-butyl methyl carbon atoms were found on a difference map and assigned to two sets with occupancies of 0.603 and 0.397, respectively. There is also disorder present in a methanolic oxygen found in two sites with occupancy factors of 0.782 and 0.218.

Physical Measurements. UV–visible spectra were obtained on a HP 8451 diode array spectrophotometer. Proton NMR spectra were obtained on an IBM WM-300 spectrometer. Deuteron NMR spectra were obtained on an IBM WM-200 spectrometer outfitted with a multinuclear

(14) Pyrz, J. W.; Roe, A. L.; Stern, L. J.; Que, L., Jr. *J. Am. Chem. Soc.* **1985**, *107*, 614–620.

(15) Cox, D. D.; Benkovic, S. J.; Bloom, L. M.; Bradley, F. C.; Nelson, M. J.; Que, L., Jr.; Wallick, D. E. *J. Am. Chem. Soc.* **1988**, *110*, 2026–2032.

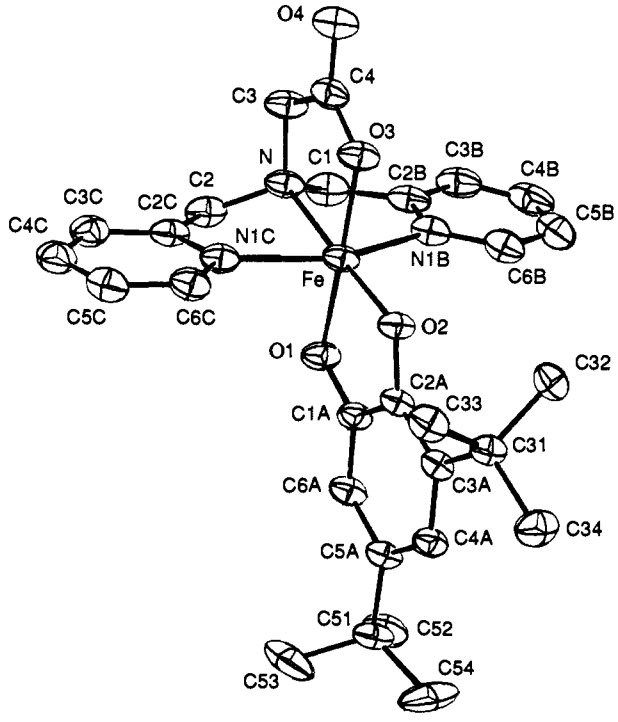

Figure 1. ORTEP plot of [Fe(BPG)DBC] showing 50% probability ellipsoids and numbering scheme. Hydrogens have been omitted for clarity.

Table III. Selected Bond Distances and Bond Angles for [Fe(BPG)DBC]·2CH_3OH

	Bond Lengths (Å)		
Fe–O1	1.989 (2)	N1B–C2B	1.353 (4)
Fe–O2	1.889 (2)	C2B–C3B	1.386 (5)
Fe–O3	1.994 (2)	C3B–C4B	1.378 (5)
Fe–N	2.218 (2)	C4B–C5B	1.393 (5)
Fe–N1B	2.147 (3)	C5B–C6B	1.366 (5)
Fe–N1C	2.140 (3)	C6B–N1B	1.345 (4)
C1A–O1	1.356 (3)	C2B–C1	1.498 (5)
C2A–O2	1.355 (3)	C1–N	1.479 (4)
C1A–C2A	1.405 (4)	N1C–C2C	1.347 (4)
C2A–C3A	1.398 (4)	C2C–C3C	1.384 (4)
C3A–C4A	1.413 (4)	C3C–C4C	1.392 (4)
C4A–C5A	1.400 (4)	C4C–C5C	1.373 (4)
C5A–C6A	1.386 (4)	C5C–C6C	1.372 (5)
C6A–C1A	1.393 (4)	C6C–N1C	1.351 (4)
O3–C4	1.292 (3)	C2C–C2	1.507 (4)
C4–O4	1.233 (3)	C2–N	1.483 (4)
C4–C3	1.522 (4)	C3–N	1.498 (3)
	Bond Angles (deg)		
N–Fe–O1	95.9 (1)	Fe–N–C1	108.9 (2)
N–Fe–O2	177.1 (1)	Fe–N–C2	106.8 (2)
N–Fe–O3	82.7 (1)	Fe–N–C3	105.4 (2)
N–Fe–N1B	76.7 (1)	Fe–O3–C4	118.0 (2)
N–Fe–N1C	76.3 (1)	Fe–N1B–C2B	116.7 (2)
O1–Fe–N1B	90.7 (1)	Fe–N1B–C6B	124.1 (2)
N1B–Fe–O3	89.6 (1)	Fe–N1C–C2C	116.6 (2)
O3–Fe–N1C	90.1 (1)	Fe–N1C–C6C	124.5 (2)
N1C–Fe–O1	89.0 (1)	O1–C1A–C2A	116.8 (2)
O1–Fe–O2	83.8 (1)	O2–C2A–C1A	115.1 (2)
Fe–O1–C1A	110.0 (2)	Fe–O2–C2A	114.2 (2)

probe. Electrochemical measurements were obtained in DMF with 0.1 M tetrabutylammonium tetrafluoroborate using a BAS100 electrochemical analyzer with a Pt working electrode and an SCE reference electrode. The ferrocenium/ferrocene couple was measured under the same conditions to enable future corrections for junction potentials (+0.465 V).[16]

Oxygenation Studies. Reactivity studies were performed in DMF with tenfold piperidine relative to complex in an oxygen atmosphere under ambient conditions. Typically, 0.1 mmol of complex was reacted with O_2 in 20 mL of solvent. After the reaction was complete, as indicated

(16) Gagne, R. R.; Koval, C. A.; Lisensky, G. C. *Inorg. Chem.* **1980**, *19*, 2854–2855.

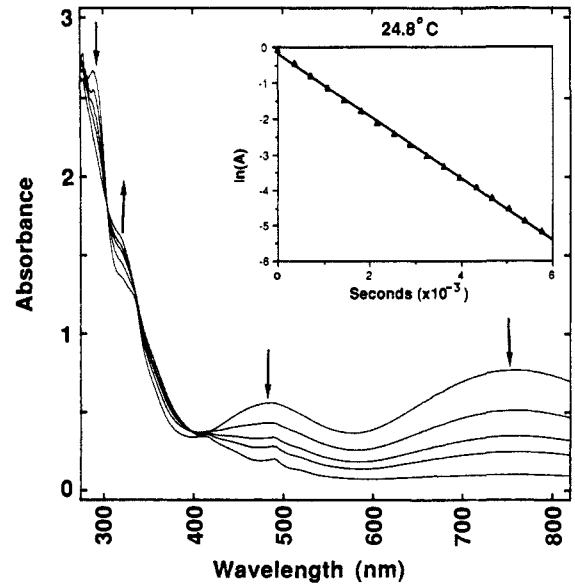

Figure 2. Progress of the reaction of [Fe(BPG)DBC] in DMF with O_2 as monitored by visible spectroscopy at 0, 6, 12, 18, and 40 min. Inset: plot of ln A vs t for the [Fe(BPG)DBC] reaction at 24.8 °C.

Table IV. Structural Parameters of the Glycine–Fe–DBC Plane in [Fe(L)DBC] Complexes

r (Å)	L = BPG[a]	L = NTA[b]
Fe–O(DBC)	1.989 (2)	1.979 (3)
Fe–O′(DBC)	1.889 (2)	1.887 (3)
Fe–N(amine)	2.218 (2)	2.224 (3)
Fe–O(OOC)	1.994 (2)	2.002 (3)
C–O(DBC)	1.356 (3)	1.338 (5)
C′–O′(DBC)	1.355 (3)	1.349 (5)
C–C′(DBC)	1.405 (4)	1.424 (6)

[a] This work. [b] Reference 13.

by the loss of color due to the catecholate LMCT bands, the solution was acidified with HCl to pH 3. Organic products were extracted from the aqueous DMF solution with diethyl ether (3 × 100 mL), dried over anhydrous $MgSO_4$, and then concentrated. The product mixture was then subjected to reverse-phase isocratic HPLC separation (Waters 6000A isocratic system; Kratos 769Z variable wavelength detector, 240 nm; Whatman Partisil ODS-5 C18 column) with a solvent mixture consisting of $CH_3CN/CH_3OH/H_2O/CH_3COOH$ (33:33:33:1). The products eluted were compared with known standards where possible.

Kinetic studies were performed on an HP-8451 diode array spectrophotometer with temperature control by an Endocal RTE-5 refrigerated circulating bath. Oxygen was bubbled through the solution (0.5–0.8 mM in complex) and then maintained at 1 atm of pressure above the reacting solution.[17] The oxygenation kinetics was followed by monitoring the disappearance of the lower energy charge transfer band of the DBC complexes (Figure 2).

Results

Crystal Structure of [Fe(BPG)DBC]·2CH_3OH. The crystal structure of [Fe(BPG)DBC] (Figure 1) closely resembles that found for $[Fe(NTA)DBC]^{2-}$ (see Table IV for a comparison).[13] Both complexes are distorted octahedra with approximate C_s symmetry, the glycine portion of the tetradentate ligand and the catecholate defining the approximate plane of symmetry. Like $[Fe(NTA)DBC]^{2-}$, [Fe(BPG)DBC] exhibits an asymmetrically chelated DBC ligand with the Fe–O bond trans to the amine N (1.889 Å) being 0.1 Å shorter than that trans to the carboxylate O (1.989 Å). This difference in bond lengths, much larger than the esd's, is due, at least in part, to a trans effect where the catecholate oxygen with the shorter bond in trans to the much weaker amine ligand. The electronic effect of the *tert*-butyl groups also appears important. A comparison of the pK_a's of 3,5-di-

(17) The solubility of O_2 in DMF was obtained from a 1957 DuPont Engineering Department research report entitled, Solubility in DMF of Acetylene and Other Gases Obtained in the Wulff Process.

Table V. A Comparison of the Properties of [Fe(L)DBC] Complexes in DMF

L	λ_{max} (nm)	$E^{o\prime}$(DBSQ/DBC) (mV vs SCE)	δ (ppm) (DBC 6- & 4-H)	$k(10^{-2}$ M^{-1} $s^{-1})$ (25 °C)
HDP	476, 726	+241	30, 16	0.33
NTA	414, 620	+24	19, 14	1.6
PDA	440, 682	+255	16, 9	4.2
BPG	488, 762	+342	8, -18	17.8

tert-butylphenol and 2,4-di-*tert*-butylphenol, 10.3 and 11.7, respectively, indicates that the protonated O2 oxygen of 3,5-di-*tert*-butylcatechol is the weaker acid.[18] As such, its conjugate base should be the stronger ligand and afford a stronger interaction with the iron center. As with $[Fe(NTA)DBC]^{2-}$, steric interactions in [Fe(BPG)DBC] appear not to be a factor, since the more sterically hindered O2 makes the shorter Fe–O bond. Another factor in the asymmetry is the presence of hydrogen bonding from a methanol of solvation to the O1 oxygen which would be expected to lengthen the Fe–O1 bond. Indeed studies on a different crystallographic form obtained from aprotic solvents, [Fe(BPG)DBC]·CH_2Cl_2·$C_6H_5CH_3$, showed that the asymmetry of catecholate binding was still present but was less pronounced (Δr_{Fe-O} = 0.04 Å).[19]

The bond lengths found for DBC are similar to those expected for a chelated catechol; they compare favorably with those observed for $[Fe(NTA)DBC]^{2-}$,[13] $[Mn(DBC)_3]^{2-}$,[20] and [Cu(bpy)DBC].[21] The other ligating groups exhibit typical bond lengths. The Fe–O(carboxylate) bond is 1.994 (2) Å, somewhat shorter than those found in $[Fe(NTA)DBC]^{2-}$ (2.002–2.039 Å),[13] reflecting the greater Lewis acidity of the iron center in [Fe(BPG)DBC]. The Fe–N(amine) bond at 2.218 (2) Å is comparable to that found for $[Fe(NTA)DBC]^{2-}$, while the Fe–N(pyridine) bonds at 2.140 (3) and 2.147 (3) Å are similar to those found for $[Fe_2O(OAc)_2(tpbn)_2]_2$·$4H_2O$ (2.142 and 2.130 Å).[22] The intraligand bond lengths are unremarkable.

It is also interesting to note that, of the three possible pendant groups, the DBC is trans to the carboxylate in [Fe(BPG)DBC] as in $[Fe(NTA)DBC]^{2-}$. The two complexes are thus simply related by a change of axial ligands relative to the DBC–Fe–glycine plane. It would appear likely that $[Fe(PDA)DBC)]^{-}$, the middle member of the series, would have a structure intermediate between the two.

Spectroscopic and Electrochemical Properties. All the DBC complexes studied exhibit EPR spectra typical of high-spin ferric complexes, with no indication of semiquinone radical signals.[15] The visible spectra of the complexes are dominated by two moderately intense bands (ϵ 1200–2500 M^{-1} cm^{-1}); they have been assigned as catecholate-to-Fe^{III} charge-transfer transitions on the basis of the extinction coefficients, the spectral shifts with various substituted catechols, and resonance Raman spectroscopy.[15] As previously noted, the positions of the two bands in the DBC complexes (Table V) are dependent upon the nature of L, with the highest energy LMCT bands arising from complexes of more Lewis basic tripodal ligands. The series NTA > PDA > BPG illustrates the effect of replacing carboxylates with pyridines. As the tripodal ligand set becomes more nitrogenous, the ferric center becomes more Lewis acidic, and the ligand–metal orbital energy gap diminishes. In this series of complexes, it is likely that there is a common tetragonal ligand set, i.e., DBC and NCH_2COO^{-}, and substitutions occur at positions normal to the Fe–DBC plane

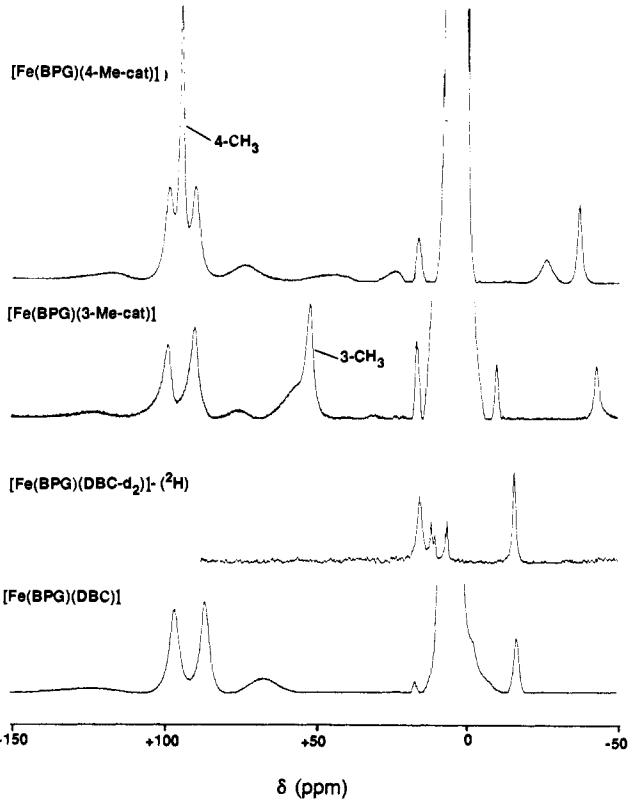

Figure 3. NMR spectra of [Fe(BPG)catechol] complexes in acetone-d_6 under ambient conditions: (a) 4-Me-cat (^{1}H); (b) 3-Me-cat (^{1}H); (c) DBC-4,6-d_2(^{2}H); (d) DBC (^{1}H).

as suggested by the crystal structures of $[Fe(NTA)DBC]^{2-}$ and [Fe(BPG)DBC]. Replacement of the carboxylate in [Fe(BPG)DBC] with a phenolate in [Fe(HDP)DBC] results in a blue shift in the LMCT bands, as would be expected for the more Lewis basic phenolate.

The electrochemistry of these complexes also reflects the interaction of the ferric center with the coordinated DBC (Table V). All the cyclic voltammograms show a redox process associated with the DBC/DBSQ couple, which ranges from +24 to +342 mV vs SCE, and is considerably more positive than the free DBSQ/DBC couple.[23] This large positive shift indicates that the coordination of the DBC to the ferric center significantly stabilizes the DBC oxidation state. The variations in the redox potential have also been noted previously and are associated with the differing Lewis acidities of the ferric centers in the complexes.[15] Interestingly, the DBSQ/DBC wave is quasireversible with the trianionic ligands but becomes increasingly less reversible as the charge of the tripodal ligand decreases. This trend probably reflects the instability of the $LFe^{III}DBSQ$ complex relative to LFe^{II} + free DBQ. Trianionic ligands would be expected to favor the Fe^{III} oxidation state, but the balance would tip toward the Fe^{II} state as L becomes more nitrogenous.

For [Fe(BPG)DBC] and [Fe(HDP)DBC], the Fe^{III}/Fe^{II} couple is also observed, since the relevant region is not obscured by redox processes associated with the cation. The feature for [Fe(HDP)DBC] is observed at −1287 mV vs SCE and is quasireversible, while that for [Fe(BPG)DBC] is at −927 mV vs SCE and essentially irreversible, the more positive value as expected for the less basic ligand.

The electrochemical data follow in general the same trend observed for the LMCT bands, where the most Lewis acidic ferric center gives rise to the lowest energy LMCT bands and the most positive potentials. The position of the HDP complex in the electrochemical series, however, differs from that in the LMCT series, which suggests that the replacement of a carboxylate group

(18) Serjeant, E. P.; Dempsey, B., Eds. *Ionization Constants of Organic Acids in Aqueous Solution*; Pergamon Press: New York, 1979; p 671.
(19) Crystal data for [Fe(BPG)DBC]·CH_2Cl_2·$C_6H_5CH_3$: space group, $C2/c$; a = 30.70 (3) Å, b = 14.50 (7) Å, c = 14.56 (7) Å, α = 90°, β = 102.3 (1)°, γ = 90°; V = 6655 Å^3, Z = 8. This structure was refined to an R value of 0.098 but was not further pursued because of the availability of the superior crystal form reported in detail in this paper.
(20) Hartman, J. R.; Foxman, B. M.; Cooper, S. R. *Inorg. Chem.* **1984**, *23*, 1381–1387.
(21) Buchanan, R. M.; Wilson-Blumenberg, C.; Trapp, C.; Larsen, S. K.; Greene, D. L.; Pierpont, C. G. *Inorg. Chem.* **1986**, *25*, 3070–3076.
(22) Toftlund, H.; Murray, K. S.; Zwack, P. R.; Taylor, L. F.; Anderson, O. P. *J. Chem. Soc., Chem. Commun.* **1986**, 191–193.
(23) Nanni, E. J., Jr.; Stallings, M. D.; Sawyer, D. T. *J. Am. Chem. Soc.* **1980**, *102*, 4481–4485.

Table VI. ^1H Chemical Shifts of Coordinated Catecholate Protons

		DBC				methyl-catechols	
L	solvent	6-H	4-H	3-*t*-Bu	5-*t*-Bu	3-Me	4-Me
NTA	DMF[a]	+19	+14				
	MeOH-d_6	+37	+22	+1.6	+5.1		
	DMSO-d_6					+39	+47
PDA	DMF[a]	+16	+9				
	MeOH-d_6	+43	+19	+1.6	+6.1		
	CD_2Cl_2	+21	−1				
	DMSO-d_6					+43	+62
BPG	DMF[a]	+8	−18				
	MeOH-d_6	+39	−2	+1.6	+7.6		
	CD_2Cl_2	+13	−23				
	DMSO-d_6					+50	+86
HDP	DMF[a]	+30	+16				
	MeOH-d_6	+57	+36	+1.9	+4.8		
	CD_2Cl_2	+34	+17				
	DMSO-d_6					+25	+47

[a] Obtained by ^2H NMR of DBC-*4,6-d*$_2$ complexes.

with the phenolate introduces a significant perturbation in the electronic structure of the iron center.

NMR Properties. The FeL(catecholate) complexes exhibit large NMR contact shifts (Figure 3, Table VI) which provide further insight into the electronic structure of the complexes. For complexes with pyridine ligands, the NMR spectra are dominated by the pyridine meta protons, which appear as relatively sharp features in the vicinity of 75–95 ppm. These shifts are approximately twice as large as those of Fe^{II} complexes of BPG and PDA in D_2O and corroborate the high-spin ferric nature of the complexes. The pyridine ortho protons are broadened due to their proximity to the metal center and difficult to observe, while the para protons resonate near the diamagnetic region and are often obscured. Additional spectral features from the complexes arise from the methylene protons, which may appear as broad features and have chemical shifts that depend on the orientation of the C–H bond relative to the orbital with unpaired spin density. The phenolate protons on the HDP complex also exhibit shifts expected for a high-spin ferric complex.

The catecholate shifts, on the other hand, exhibit a remarkable dependence on the nature of the tetradentate ligand (Tables V and VI). The DBC 4-H and 6-H protons for complexes in DMF solution exhibit shifts that range from +30 and +16 ppm for Fe(HDP)DBC to +8 and −18 ppm for Fe(BPG)DBC. (Since the DBC 4-H and 6-H protons were sometimes difficult to observe in the ^1H spectrum, the DBC ligand was selectively deuteriated at C-4 and C-6 and the complexes were monitored by ^2H NMR.) For all cases, the more downfield shifted resonance is the broader of the two protons and thus assigned to the 6-H proton because of its proximity to the metal center. There appears to be a general upfield shift from the downfield shifted position of the HDP complex in the order HDP, NTA, PDA, and BPG. Similar trends are observed in MeOH and CH_2Cl_2 solutions.

The methyl shifts of the 3-methylcatechol and 4-methylcatechol complexes also show a dependence on the nature of the tetradentate ligand (Table VI). The difference in the methyl isotropic shifts is ca. 10 ppm for the NTA complex and increases to ca. 20 ppm for the PDA complexes and ca. 40 ppm for the BPG complexes. A similar trend is observed for the *tert*-butyl protons on the DBC complexes, although the effect is much smaller because of the attenuation of the contact shift through the σ bonds.

The catecholate shift patterns observed in these complexes differ from those expected from previous observations on iron(III)–phenolate complexes.[14,24] The DBC shifts observed for the NTA and HDP complexes are downfield as expected from the phenolate model. The bidentate nature of the DBC coordination gives rise to two opposing delocalization pathways via O1 and O2. Spin delocalization via O1 should shift the 4- and 6-H resonances upfield because they are ortho and para to O1, while delocalization via O2 should shift them downfield because they are meta to O2. The crystal structures of DBC complexes show that the Fe–O2 bond is significantly shorter than the Fe–O1 bond, so the O2 delocalization is expected to be dominant, thus the downfield shifts. On the basis of the iron(III)–phenolate model, the DBC resonances would be expected to shift further downfield as the LMCT bands red-shifted. This is clearly not the case, and for the BPG complex the DBC 4-H resonance is upfield-shifted.

The pattern of shifts for the 3- and 4-methyl protons of the 3-Me-cat and 4-Me-cat complexes of the series also differs from that expected from the phenolate model.[14] On the basis of this model, the methyl shifts should be comparable in magnitude and should increase as the LMCT bands are red-shifted. In phenolate complexes, ortho and para methyl shifts are both downfield and comparable in magnitude but significantly larger than meta methyl shifts that are upfield; thus the combination of two competing spin delocalization pathways (i.e., meta vs ortho shifts for the 3-methyl group and meta vs para shifts for the 4-methyl group) results in equivalent downfield shifts for both. However, for the series of complexes in this study, the 4-methyl shift progressively becomes larger than the 3-methyl shift as the iron center becomes more Lewis acidic. A similar trend is also observed for the 3- and 5-*tert*-butyl resonances.

The trends exhibited by the catecholate isotropic shifts as the LMCT shifts to lower energy suggest that the phenolate model is inadequate to explain the shifts observed. We propose that the pattern of shifts observed arises from an increased semiquinone character for the coordinated catecholate as the metal center becomes more Lewis acidic, i.e., an increased contribution from the Fe^{II}–semiquinone form to the predominant Fe^{III}–catecholate description. It is clear from the properties of the complexes that the best ground-state description of the complexes is that of a catecholate coordinated to a high-spin ferric center.[15] The EPR spectra are readily interpreted within the framework of an $S = {}^5/_2$ spin Hamiltonian, and no observable signal assignable to a semiquinone species is observed. The dominant ferric character of the complexes is also indicated by the ferric-like shifts of the tetradentate ligand, and the crystal structures of the two DBC complexes clearly show the catecholate character of the benzenediolate ligand.[25] However, a small contribution of the Fe(II)–semiquinone form to the description of the complexes, while leaving the structural parameters and EPR spectra virtually unperturbed, would significantly affect the observed catecholate shifts because of the sensitivity of the paramagnetic shift to the entailed changes in unpaired spin density and distribution.

The trends in the isotropic shifts as a function of the tripodal ligand serve to support this model. MO calculations show that the orbital that contains the unpaired electron in a semiquinone has large coefficients at C-4 and C-5 and very small values at C-3 and C-6.[26] This is corroborated by EPR studies of DBSQ where only hyperfine splittings for the 4-H and the 5-*tert*-butyl protons are observed.[27] Thus the increasingly larger shifts for the 4-methyl protons of the 4-methylcatechol complexes relative to their 3-isomers reflects the much larger spin density at C-4 vs C-3, consistent with greater semiquinone character. The same argument also applies to the difference in *tert*-butyl shifts observed in the DBC complexes.[28] The trends exhibited by the DBC ring protons reflect the switch in the sign of a_H when a ring C–H is replaced by an alkyl group. So increased semiquinone character that gives rise to larger downfield shifts for the C-4 and C-5 alkyl protons should give rise to upfield shifts for the corresponding ring protons.

(24) Heistand, R. H.; II; Lauffer, R. B.; Fikrig, E.; Que, L., Jr. *J. Am. Chem. Soc.* **1982**, *104*, 2789–2796.

(25) Pierpont, C. G.; Buchanan, R. M. *Coord. Chem. Rev.* **1981**, *38*, 44–87.

(26) Kahn, O.; Prins, R.; Reedijk, J.; Thompson, J. S. *Inorg. Chem.* **1987**, *26*, 3557–3561. Yamabe, S.; Minato, T.; Kimura, M. *J. Phys. Chem.* **1981**, *85*, 3510–3513.

(27) Trapp, C.; Tyson, C. A.; Giacometti, G. *J. Am. Chem. Soc.* **1968**, *90*, 1394–1400.

(28) A similar differentiation in *tert*-butyl NMR shifts is reported for [Co(DBSQ)$_2$bpy] in a paper by Pierpont and Buchanan (Pierpont, C. G.; Buchanan, R. M. *J. Am. Chem. Soc.* **1980**, *102*, 4951–4957).

Table VII. Reactivity and Kinetic Data for [Fe(L)DBC] Complexes

complex	% furanone[a]	k^b(DMF)	k^b(CH_3OH)	k^b(CH_2Cl_2)	$\Delta H^{\ddagger}$ [c]	$\Delta S^{\ddagger}$ [c]
[Fe(HDP)DBC]	91	0.33	0.49	0.81		
$[Fe(NTA)DBC]^{2-}$	84	3.7	1.0	*d*	12.8	−22
$[Fe(PDA)DBC]^{-}$	95	4.3	5.0	3.7	11.4	−27
[Fe(BPG)DBC]	97	18.3	42.6	36.6	10.2	−28
[Ga(BPG)DBC]	4					

[a] Reactions run in DMF under 1 atm of O_2 in the presence of a tenfold excess of piperidine until the LMCT bands had disappeared. The Ga complex was treated under the same conditions as [Fe(BPG)DBC]. Furanone refers to (3,5-di-*tert*-butyl-2-furanon-5-yl)acetic acid amides.[13] [b] In units of 10^{-2} M^{-1} s^{-1}. [c] In DMF solution; units of kcal/mol for $\Delta H^{\ddagger}$, and cal/(deg·mol) for $\Delta S^{\ddagger}$. [d] Data not obtained due to lack of solubility.

Reactivity and Kinetics. The [FeL(DBC)] complexes all react with dioxygen to yield products due to the oxidative cleavage of the catechol ring, i.e.

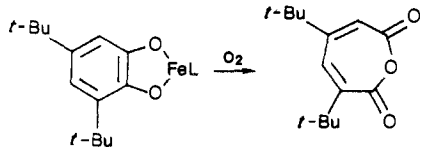

As such, they model well the reactivity of the catechol dioxygenases. Table VII summarizes the product yields, showing that the ligand environment plays a role in modulating the reactivity of these complexes. Previous work from this laboratory involving tripodal ligands with three pendant oxy-anion ligating functionalities has demonstrated that the yield of intradiol cleavage product increases as the Lewis acidity of the metal center increases.[13] In this work, we have extended our investigations to complexes with even more Lewis acidic ferric centers and obtain an even greater specificity for the intradiol cleavage reaction. The BPG complex reacts with O_2 to give a 97% yield of the desired product and in a significantly shorter period of time than the corresponding NTA complex.

We have also prepared [Ga(BPG)DBC] in order to test the requirement for a paramagnetic center. Gallium(III) is a d^{10} metal ion with an ionic radius similar to that of iron(III), 0.62 vs 0.645 Å, respectively;[29] thus, Ga^{III} would be expected to have a Lewis acidity similar to that of Fe^{III}.[30] Under the same reaction conditions and workup procedures, the yield of cleavage product from the Ga complex was significantly less than that for the Fe complex, indicating that factors in addition to Lewis acidity affect the reactivity of the model complexes.

The uniformly high specificities of the complexes in this study have allowed the study of the kinetics for the oxidative cleavage reaction (Table VII). The kinetics of the reaction with dioxygen can be followed by monitoring the disappearance of the lower energy catecholate LMCT band at 25 °C (Figure 2). Exposure of the complex to O_2 does not alter the visible spectral properties of the solution, save for the exponential decrease in intensity with time. The reactions all exhibit pseudo-first-order kinetics under conditions where dioxygen was in excess with the time courses remaining linear over 5 half-lives (for an example, see Figure 2 inset); the pseudo-first-order rate constants further showed a first-order dependence on dioxygen concentration (investigated only for the [Fe(BPG)DBC] reaction). The rates of the reactions increase in the order HDP < NTA < PDA < BPG in all solvents studied (Table VII). Activation parameters were determined for the oxygenation reactions of $[Fe(NTA)DBC]^{2-}$, $[Fe(PDA)DBC]^{-}$, and [Fe(BPG)DBC] in DMF (Table VII); as an example, the plot of ln (k/T) vs $1/T$ over the range of −3 to 46 °C for the [Fe(BPG)DBC] reaction in DMF is shown in Figure 4. The $\Delta H^{\ddagger}$ values decrease in the order NTA > PDA > BPG, similar to the relative rates of reaction, and the $\Delta S^{\ddagger}$ values are large and negative, suggestive of a bimolecular transition state. For comparison, activation parameters for the reaction of [Fe(BPG)DBC] and O_2 in MeOH were found to be 7.2 kcal mol^{-1} and −37 cal mol^{-1} K^{-1}, respectively.

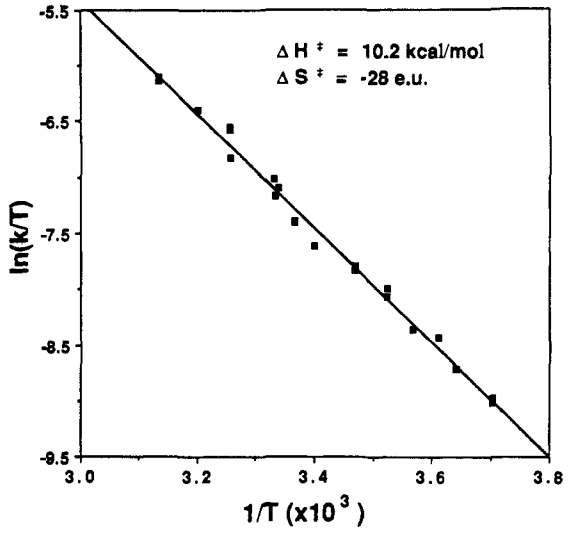

Figure 4. Plot of ln (k/T) vs $1/T$ for the reaction of [Fe(BPG)DBC] and O_2 in DMF where k represents the second-order rate constant for the reaction.

Discussion

In a previous paper, we reported an investigation of the dioxygen reactivity of $[Fe(L)DBC]^{2-}$ complexes, where L represented a series of trianionic tripodal ligands.[13] These complexes were found to react with O_2, yielding varying amounts of intradiol cleavage product that increased as the ferric center became more Lewis acidic. These observations provided the first insights into the role of the iron center in the oxygenation reaction, particularly in coordinating the intermediate peroxide and thereby directing the regiospecificity of dioxygen attack. We have extended our study of [Fe(L)DBC] complexes to include tripodal ligands that further enhance the Lewis acidity of the ferric center. The latter complexes react with O_2 faster and give rise to nearly quantitative yields of the desired product, constituting the most specific of the oxidative cleavage systems in the literature. These observations allow us to further refine the proposed oxidative cleavage mechanism and gain insight into the nature of the substrate activation step.

The kinetic studies show that the rate of reaction for [Fe(BPG)DBC] is 5–40 times faster than that for $[Fe(NTA)DBC]^{2-}$. Their crystal structures indicate, however, that the iron coordination environments are very similar. In particular, the iron(III)–catecholate interactions in the two complexes as indicated by the Fe–O(DBC) bond lengths are almost identical. In both cases, the Fe–O2 bond is shorter than the Fe–O1 bond by nearly 0.1 Å; the large difference in the bond lengths reflects the stronger basicity of O2 and the weakness of the Fe–N bond trans to O2. The DBC ligand also coordinates trans to the glycine moiety of the tripodal ligand in both structures. It has been proposed that the asymmetric coordination of the DBC gives rise to a monodentate DBC in the activated complex capable of reaction with

(29) Shannon, R. D. *Acta Crystallogr. Sect. A* **1976**, *A32*, 751–767. Borgias, B. A.; Barclay, S. J.; Raymond, K. N. *J. Coord. Chem.* **1986**, *15*, 109–123.

(30) For example, the equilibrium constants for the following reaction, $[M(H_2O)_6]^{3+} \rightleftharpoons [M(H_2O)_5OH]^{2+} + H^+$, are comparable for Fe (8.9×10^{-4}) and Ga (2.5×10^{-3}): Cotton, F. A.; Wilkinson, G. *Advanced Inorganic Chemistry*, 4th ed.; John Wiley & Sons: New York, 1980, p 758. Wilkinson, G., Ed. *Comprehensive Coordination Chemistry*; Pergamon Press: Oxford, 1987; Vol. 3, p 133.

O_2.[13,31] As the BPG complex reacts faster than the NTA complex, this earlier notion would suggest that the asymmetry should be more pronounced in the former complex. The similarity of the two structures suggests that the asymmetry of the DBC coordination is less important than earlier proposed and other factors must be considered in formulating a mechanism for the observed reactivity of these complexes.

The [Fe(L)DBC] complexes exhibit UV–vis, electrochemical, and NMR properties that depend on the tripodal ligand (Table V). The complexes of NTA, PDA, and BPG appear to constitute a series with a common glycine–Fe–DBC plane and varying axial ligands. This order is retained in the energies of the LMCT bands, the positions of the DBSQ/DBC couple, and the observed NMR shifts and can be understood in terms of the increasing Lewis acidity of the ferric center. When the HDP complex is interpolated into this series, it appears in different positions depending on the property being correlated. This inconsistency is probably a consequence of the phenolate replacement for carboxylate in BPG and its attendant perturbations of the iron electronic structure. When the various physical observables are compared with the relative rates of reaction, it is clear that the best predictor of relative reactivity is the NMR shifts of the catecholate. We have argued that the shifts exhibited by the Fe^{III}–catecholate complex are indicative of some contribution of an Fe^{II}–semiquinone resonance form in the electronic description of the complex. The amount of semiquinone character involved is readily manifested by the NMR shifts because of their sensitivity to differences in unpaired spin density and is enhanced in the order HDP < NTA < PDA < BPG. This order is retained when comparing relative reaction rates; the data thus indicate that the greater the semiquinone character in the complex, the faster it reacts with dioxygen.

Kinetic studies of the reactions show a dependence on the concentrations of both the complex and dioxygen. The simplest reaction sequence consistent with these observations is

$$M + O_2 \rightleftharpoons MO_2 \rightarrow \text{products}$$

where M represents the DBC complex and MO_2 is a putative oxygenated intermediate. Exposure of the DBC complexes to O_2 simply results in the gradual decrease of the spectral features due to the DBC complexes (Figure 2), and the MO_2 intermediate does not appear to accumulate. Given the large and negative activation entropies (−22 to −37 eu) found for the oxygenation reaction, it would appear that the attack of O_2 on the DBC complex is the rate-determining step. For comparison, the binding of O_2 to the binuclear copper complex, $[Cu_2(XYL–O)]^+$, has an activation entropy of −35 eu.[32]

How may the attack of O_2 on the complex occur? It should be noted that the complexes in question are six-coordinate and clearly high-spin ferric in nature; they therefore lack an open coordination site for O_2 binding and are unlikely to provide the reducing equivalents necessary to stabilize the coordination of O_2, even if such a site were available. We have thus proposed a novel substrate activation mechanism for this reaction,[8] but the nature of this activation has been a rather nebulous feature of the mechanism. Our present results indicate that increased reactivity is observed in complexes with the more Lewis acidic metal centers; however, the Lewis acidity of the metal center alone does not facilitate the reaction as demonstrated by a comparison of the relative reactivities of [Fe(BPG)DBC] and the corresponding Ga^{III} complex. What distinguishes Fe^{III} from Ga^{III} is its redox properties, and evidence that they play an important role in the mechanism is found in the NMR spectra of the complexes.

The NMR properties of the complexes indicate that the coordinated DBC ligand has semiquinone character. The semiquinone character is a result of the covalency of the iron(III)–catecholate bond, which is enhanced as the Lewis acidity of the metal center increases. A comparison of the complexes shows that the extent of radical character on the coordinated DBC correlates with the reactivity of the complexes. We thus propose that the radical character facilitates the attack of O_2 on substrate generating a transient peroxy radical, which is in turn reduced by the nascent Fe^{II} center, forming the intermediate Fe^{III}–peroxide complex, i.e.

Scheme II

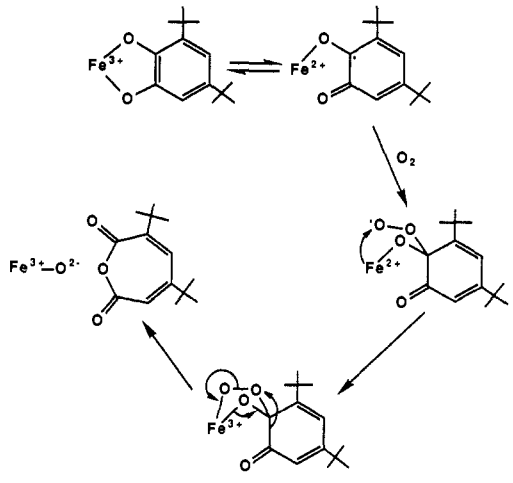

$$Fe^{III}\text{–DBC} \rightarrow Fe^{II}\text{–DBSQ} \rightarrow Fe^{II}\text{–ROO}^{\bullet} \rightarrow Fe^{III}\text{–OOR}$$

Alternatively, O_2 could bind to the Fe^{II} center, forming an Fe^{III}–DBSQ–superoxide complex; the semiquinone and superoxide would then couple to form the peroxide–Fe^{III} complex, i.e.

$$Fe^{III}\text{–DBC} \rightarrow Fe^{II}\text{–DBSQ} \rightarrow O_2\text{–}Fe^{II}\text{–DBSQ} \rightarrow O_2^{\bullet-}\text{–}Fe^{III}\text{–DBSQ} \rightarrow Fe^{III}\text{–OOR}$$

We prefer the first alternative, because both the reaction of semiquinone with O_2[33] and the reduction of the peroxy radical[33,34] are facile reactions, while the coupling of semiquinone with superoxide required by the second alternative has yet to be demonstrated.[33]

It should be emphasized that the Fe^{II}–semiquinone character ascribed to these complexes can thus far only be deduced from the NMR shifts of the catecholate ligand. The EPR spectra at 4 K,[15] the visible spectra,[15] and the NMR shifts of the pyridine protons all indicate that the complexes are best described as Fe^{III}–DBC species. These observations contrast those of Funabiki on the $FeCl_3$/bpy/pyridine system where equimolar amounts of Fe^{II} and Fe^{III} are found in the Mössbauer spectrum of the mixture after addition of $DBCH_2$.[35] The ferrous component may arise from DBC-to-Fe^{III} electron transfer in a complex with FeN_4DBC coordination, which would favor formation of an Fe^{II}–DBSQ species. As would be expected from our correlations of semiquinone character with reactivity, this mixture reacts with O_2 significantly faster than [Fe(BPG)DBC], but it is much less specific for intradiol cleavage.

The model studies reported here permit us to further refine the substrate activation mechanism proposed for the dioxygenases.[8,9,13] In previous papers, we proposed that substrate activation may involve the conversion of the bidentate catecholate to a monodentate species, thereby rendering the catecholate a better reductant and affording a site for coordinating the reduced dioxygen species. Support for this proposal has been presented by Whittaker and Lipscomb in binding studies of the transition-state analogue isonicotinic acid *N*-oxide to protocatechuate 3,4-dioxygenase;[36] they suggest that the analogue coordinates in a monodentate

(31) White, L. S.; Nillson, P. V.; Pignolet, L. H.; Que, L., Jr. *J. Am. Chem. Soc.* **1984**, *106*, 8312–8313.
(32) Karlin, K. D.; Zuberbuhler, A., unpublished observations. Karlin, K. D.; Cruse, R. W.; Gultneh, Y.; Farooq, A.; Hayes, J. C.; Zubieta, J. *J. Am. Chem. Soc.* **1987**, *109*, 2668–2679.
(33) White, L. S.; Que, L., Jr. *J. Mol. Catal.* **1985**, *33*, 139–149.
(34) Sheldon, R. A.; Kochi, J. K. *Metal-Catalyzed Oxidations of Organic Compounds*; Academic: New York, 1981; p 45. Ingold, K. V. *Acc. Chem. Res.* **1969**, *2*, 1–9.
(35) Funabiki, T.; Tada, S.; Yoshioka, T.; Takano, M.; Yoshida, S. *J. Chem. Soc., Chem. Commun.* **1986**, 1699–1700.
(36) Whittaker, J. W.; Lipscomb, J. D. *J. Biol. Chem.* **1984**, *259*, 4476–4486.

fashion to the ferric center via the *N*-oxide oxygen, leaving the other exogenous ligand coordination site accessible to a solvent molecule. Our current studies suggest that the monodentate coordination in the activated substrate may result from electron transfer from the catecholate to the ferric center yielding a ferrous–semiquinone complex (Scheme II); such a complex would allow the C–O and O–Fe bonds to form in rapid succession, yielding the intermediate peroxide complex. In this proposed mechanism, the ketonized isonicotinate *N*-oxide would be a close steric and electronic analogue to the putative monodentate semiquinone, i.e.

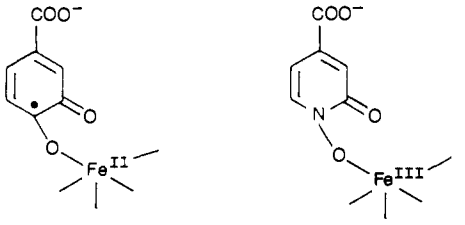

The synthetic complexes we have discussed serve as good functional mimics for the dioxygenase-catalyzed oxidative cleavage of catechols to the extent that an Fe^{III}–catecholate complex reacts with O_2 to yield specifically the intradiol cleavage product as dictated by the experimental observations on the enzymes. However, there is still a long way to go toward a full understanding of the enzyme–substrate complex and its reaction with O_2. First, it is of interest to note that, while the synthetic complex of the tripodal ligand with one phenolate is the slowest reacting of the complexes studied, the dioxygenases have active sites with *2* tyrosines coordinated to the iron center.[1,37] Second, though the synthetic complexes exhibit visible and Raman spectral features that grossly mimic those of the dioxygenase ES complexes, i.e., the presence of low-energy catecholate-to-Fe^{III} charge-transfer transitions, the model complexes do not simulate the spectral shape of the ES complexes well. Most importantly, the ES complexes react with O_2 six orders of magnitude faster[7] than [Fe(BPG)DBC]. Clearly, the dioxygenase active site possesses features yet to be duplicated in the models. What features are missing may become apparent with a careful scrutiny of the active site as crystallographic studies of protocatechuate 3,4-dioxygenase from *Pseudomonas aeruginosa* unfold.[37]

Acknowledgment. This work has been supported by the National Institutes of Health (GM-33162). We thank Professor Doyle Britton and Paul D. Boyle for their invaluable assistance in the crystallographic studies and Dr. A. S. Borovik for his efforts in the synthesis of the HDP ligand.

Supplementary Material Available: A listing of atomic positional parameters and thermal parameters (4 pages). Ordering information is given on any current masthead page.

(37) Ohlendorf, D. H.; Weber, P. C.; Lipscomb, J. D. *J. Mol. Biol.* **1987**, *194*, 225–227.

1,2-Didehydroazepines from the Photolysis of Substituted Aryl Azides: Analysis of Their Chemical and Physical Properties by Time-Resolved Spectroscopic Methods

Yu-Zhuo Li,[1] John P. Kirby,[1] Michael W. George,[2] Martyn Poliakoff,[2] and Gary B. Schuster*,[1]

Contribution from the Department of Chemistry, Roger Adams Laboratory, University of Illinois, Urbana, Illinois 61801, and the Department of Chemistry, University of Nottingham, Nottingham, England. *Received May 19, 1988*

Abstract: A series of substituted 1,2-didehydroazepines was prepared by photolysis of their precursor aryl azides. The chemical and physical properties of the didehydroazepines were probed by means of conventional chemical trapping experiments and by time-resolved spectroscopy with IR and UV detection. The experimental results are compared with predictions from MNDO calculations. The didehydroazepines are formed from the azides with efficiencies that depend systematically on the nature of the substituent. In some cases, didehydroazepines are not formed at all. The didehydroazepines react relatively rapidly with starting aryl azide and with added amines. The rate of their reaction is largely controlled by the electronic properties of the substituent on the didehydroazepine. These results permit prediction of the reactivity of didehydroazepines from their structure.

It is well established that irradiation of phenyl azide at room temperature in a solution containing diethylamine gives 2-(diethylamino)-3*H*-azepine in good yield[3] (eq 1). It was recognized

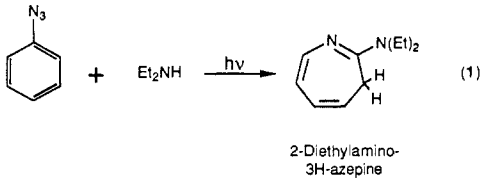

a long time ago that this reaction must proceed through a met-

Chart I

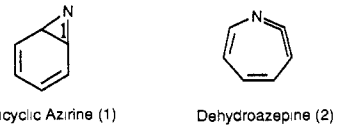

astable intermediate whose structure was formulated as either 7-azabicyclo[4.1.0]hepta-2,4,7-triene (bicyclic azirine **1**) or 1,2-didehydroazepine (**2**) (Chart I).[4] Subsequently, didehydroazepine from photolysis of phenyl azide was observed by means of infrared spectroscopy in rare-gas matrices at 8 K.[5] We recently confirmed

(1) University of Illinois.
(2) University of Nottingham.
(3) Smith, P. A. S. In *Azides and Nitrenes*; Scriven, E. F. V., Ed.; Academic: New York, 1984; p 95 ff. Doering, W. E.; Odum, R. A. *Tetrahedron* **1966**, *22*, 81.

(4) Huisgen, R.; Vossius, D.; Appl. M. *Chem. Ber.* **1958**, *91*, 1. Huisgen, R.; Appl, M. *Chem. Ber.* **1958**, *91*, 12. Sundberg, R. J.; Brenner, M.; Suter, S. R.; Das, B. P. *Tetrahedron Lett.* **1970**, 2715. Crow, W. D.; Wentrup, C. *Tetrahedron Lett.* **1968**, 6149.

0002-7863/88/1510-8092$01.50/0